Provably Safe Conflict Resolution With Bounded Turn Rate for Air Traffic Control

Jeff Yoo and Santosh Devasia

***Abstract*— This brief presents a decoupled conflict resolution procedure (CRP) for en route air traffic control. The key concept is to split the main routes into multiple paths, which results in larger spacing between aircraft for enabling conflict-free intersections. These paths are then merged back into the original route to avoid additional conflicts in the region beyond the local space needed for the CRP. The main contribution of this brief is the development of CRPs that bound the heading change (turn) rate to account for limitations arising from aircraft turn dynamics. The proposed decoupled CRPs satisfy conditions for guaranteed safety (i.e., are provably safe) and do not lead to flow-capacity loss in either of the intersecting routes. Moreover, the impact of including the bounded turn-rate limitation is studied, and issues in the applicability of the proposed CRP are illustrated.**

***Index Terms*— Air safety, air traffic control, conflict resolution procedures, distributed control, intelligent transportation systems.**

I. Introduction

THIS BRIEF presents a procedure for resolving conflicts between aircraft along intersecting routes. A challenge in the design of conflict resolution procedures (CRPs) is to guarantee the overall safety and efficiency of a route network with multiple intersections—where each CRP acts locally in space and in time. Recent work [1] has identified the necessary and sufficient local conditions on such CRPs to ensure global safety. However, this recent work [1] on the existence of such decoupled CRPs (which can be implemented in a decentralized manner) did not bound the aircraft turn rate, i.e., the heading angle was assumed to change instantly. While the roll dynamics (which leads to an aircraft turn) is relatively fast and can be ignored in the CRP design, the turn dynamics places an upper bound on the turn rate [2], which could affect the CRP design. The main contribution of this brief is to extend the design of provably safe CRPs by including the bounded turn-rate limitation. This brief builds on previous preliminary results [3], [4] by providing detailed proofs of the main results, clarifying the importance of including the turn dynamics, and illustrating issues in the applicability of the proposed CRP.

CRPs tend to be decoupled (spatially and temporally) because of a substantial increase in computational and modeling complexity with a single global CRP (due to increased number of aircraft and conflicts) when compared to decoupled CRPs, such as in [5]. Additionally, a global CRP over a large airspace is inefficient (with lower overall capacity [6]) because of the need to handle the larger uncertainty [7]. The uncertainty tends to be larger, e.g., because of ground speed sensitivity to wind and temperature, which depend, in turn, on forecasts of dynamic weather conditions with substantial uncertainties over time [8]. Therefore, decoupled CRPs are needed to manage the complexity and uncertainty in air traffic control (ATC).

It is challenging to guarantee overall stability in a route network with multiple decoupled CRPs. In particular, a challenge is to ensure that modifications of flight trajectories, for resolving a local conflict, do not lead to a domino effect, i.e., resolution of a conflict should not lead to new conflicts, whose resolution again leads to additional conflicts, and so on [9]. Moreover, for guaranteeing safety, the procedure should always lead to a solution of the conflict resolution problem. Developing such provably safe decoupled CRPs remains a challenging problem in ATC, which is is addressed in this brief.

Previous works on CRPs range from nonlocal probabilistic approaches that handle uncertainties [10] to local deterministic approaches that resolve conflicts in a collaborative manner [11], [12]. Analytical issues such as proving local safety of conflict resolution were studied in, e.g., [13]. Moreover, conditions for CRP stability were studied, for two and three intersecting routes, in [12] and [14]. The main difficulty is that conflict resolution at one route intersection will interact with the conflict resolution at the next intersection along a route; stable solutions to the resulting coupled problem require centralized solutions [14]. In contrast, this brief seeks decoupled procedures that guarantee conflict resolution with multiple conflicts (intersections) by using decoupled CRPs—the cost of this guarantee is time delay in the flow, however, with known bounds. An advantage of the proposed decoupled approach is that the CRP at the next intersection (along a route) can be designed independently of the current CRP. Moreover, the proposed CRP does not require a reduction of the flow capacity in each route; therefore, it can aid in increasing the efficiency of en route ATC, e.g., in the design of capacity-maintaining protocols for adverse weather rerouting [1].

This brief begins with an overview of the proposed CRP in Section II, followed by the development of design conditions to ensure safety in Section III. The importance of including turn-rate bounds in the CRP design is investigated in Section IV. The proposed approach is illustrated with an example application in Section V, followed by conclusions in Section VI.

II. CRP

A. Airspace and Conflict Description

The CRP is studied for perpendicularly intersecting aircraft routes, which can occur, in highway-like route

Manuscript received February 16, 2012; revised October 22, 2012; accepted December 11, 2012. Manuscript received in final form December 19, 2012. Date of publication January 17, 2013; date of current version October 15, 2013. Recommended by Associate Editor M. Prandini.

The authors are with the University of Washington, Seattle, WA 98195-2600 USA (e-mail: jdsy@uw.edu; devasia@uw.edu).

Color versions of one or more of the figures in this paper are available online at http://ieeexplore.ieee.org.

Digital Object Identifier 10.1109/TCST.2012.2236328

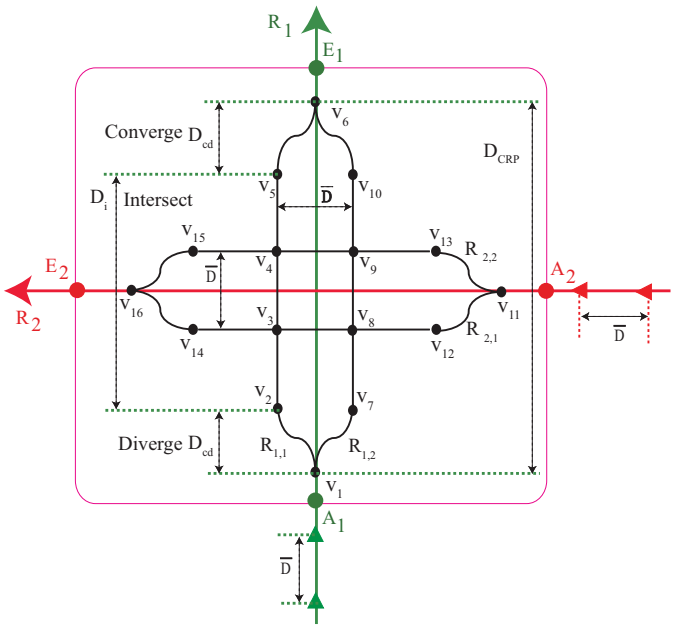

Fig. 1. Local region L of the airspace around two perpendicularly intersecting routes, R_1, R_2, the corresponding arrival points A_1, A_2, and exit points E_1, E_2. The steps of the CRP include: 1) diverge; 2) intersect; and 3) converge.

structures [15], [16]. These routes, if sufficiently dense in the airspace and variable over time [17], could provide the flexibility needed for accommodating varying weather patterns, missed connections, and traffic congestion by choosing different flight segments in a free-flight like setting while maintaining a structure for the aircraft routes. As in previous works, the intersections and routes are assumed to be at a fixed altitude (planar flight) as illustrated in Fig. 1.

Moreover, the intersections are assumed to be spatially sparse, leading to a sufficiently large local region L, around each intersection conflict point (CP), where the local region L is conflict-free from all other routes and other CPs in the airspace. The CRP can use this local region L to resolve conflicts at the intersection without potentially causing additional conflicts as long as the route modifications due to CRP procedures are contained within the local region L. Aircraft along the nominal routes (R_1 and R_2) arrive in this local region L at arrival points A_1, A_2 with a fixed nominal speed v_{sp} and exit at E_1, E_2, as shown in Fig. 1. It is assumed that aircrafts arriving at the local region L are separated by at least the distance $\overline{D}$ at the arrival points A_1, A_2, where the minimal arrival spacing $\overline{D}$ is greater than the minimum required separation distance D_{sep} to avoid conflicts.

B. Conflict Resolution Problem

The requirements on each decentralized CRP, to enable decoupled designs, are stated below.

Definition 1 [CRP Decoupling Conditions]: The problem is to find a CRP using heading change maneuvers (with bounds on the rate of heading change) such that conflicts are avoided between aircraft. The following CRP-decoupling conditions are satisfied.

1) *Local Intent:* aircraft on each route (R_1, R_2) exit along the same route at the corresponding exit point E_1, E_2.
2) *Local Liveness:* aircraft on each route exit the local region L within a specified bounded maximum time $T < \infty$.
3) *Local Fairness:* the passage through the local region L is first-come-first-served (FCFS) within each route.
4) *Local Exit Spacing:* aircraft exiting the local region L (at each point E_1, E_2) are separated by the least distance $\overline{D}$.

Remark 1: The local liveness condition implies that aircraft will not be stuck in the airspace (e.g., in a loop), and the fairness first-come, first-served (FCFS) condition facilitates acceptance of the CRP since the FCFS scheduling of aircraft through an airspace is considered as the canonical fair schedule in ATC.

Remark 2: In general, conflict resolution can be achieved using maneuvers that change the heading, speed, and altitude. However, heading changes are preferred over speed changes, which require additional fuel for accelerating and decelerating the aircraft. Similarly, heading changes are preferred over altitude changes, which tend to incur passenger discomfort and can cause conflicts in the other altitudes.

C. Proposed CRP

When aircraft are closely spaced in the intersecting routes, sufficient space might not be available for aircraft to pass through the intersection point without conflicts. In this scenario, the proposed CRP splits aircraft in each route route (using diverge procedures) into multiple paths—with increased spacing between aircraft in each path. Aircraft in these paths (with sufficiently large spacing between aircraft) can then pass through the intersection without conflicts as shown in [1]. After the intersections, aircraft in the different paths are merged back to the original routes.

Remark 3: This brief addresses perpendicular intersections. However, the main concept of splitting the route to increase aircraft spacing, followed by a merge, could be extended to nonperpendicular intersections (e.g., Lemma 5, [1]). Moreover, the current CRP can be applied to nonperpendicular cases if the routes can be rearranged to create a perpendicular intersection. This might not be possible if the intersecting routes are close to being parallel, in which case a redesign of the overall route structure might be needed.

An example CRP (with a two-path split) is shown in Fig. 1. It consists of splitting of each route (R_1, R_2) into two paths of equal length and choosing one of the paths for each arriving aircraft. In particular, the two paths $\{R_{1,i}\}_{i=1}^{i=2}$ for route R_1 (shown in Fig. 1) are described by a set of way points (v_i)

$$\begin{aligned} R_{1,1} &= \{v_1, v_2, v_3, v_4, v_5, v_6\} \\ R_{1,2} &= \{v_1, v_7, v_8, v_9, v_{10}, v_6\} \end{aligned} \tag{1}$$

and the two paths $\{R_{2,i}\}_{i=1}^{i=2}$ for route R_2 are

$$\begin{aligned} R_{2,1} &= \{v_{11}, v_{12}, v_8, v_3, v_{14}, v_{16}\} \\ R_{2,2} &= \{v_{11}, v_{13}, v_9, v_4, v_{15}, v_{16}\}. \end{aligned} \tag{2}$$

Definition 2 [Cyclic Path-Assignment Procedure]: Let the scheduled time of arrival (STA) of aircraft at the initial way

points (v_1 for route R_1 and v_{11} for route R_2 in Fig. 1) be at discrete time instants

$$t_k = k\left(\frac{\overline{D}}{v_{\rm sp}}\right) = kT_{\overline{D}} \tag{3}$$

where the index k is a nonnegative integer. Then, assign paths $R_{1,1}$ and $R_{2,1}$ (for routes R_1 and R_2, respectively) if k is odd, and paths $R_{1,2}$ and $R_{2,2}$ if k is even.

Remark 4: The time difference $2T_{\overline{D}}$ in (3) between two STAs on a single route corresponds to the time needed to travel (with nominal speed $v_{\rm sp}$) the minimum separation distance $\overline{D}$ between aircraft arriving in each route.

Remark 5 (Decentralized Implementation): Although the design of the route structure and the CRPs and the availability of a global clock are centralized, aircraft can self-select (without collaboration) the CRP path based on the arrival time index t_k. In this sense, the CRP can be implemented in a decentralized manner—this is similar to automobiles following traffic light rules in a decentralized fashion. Tight control over the space–time trajectories of the aircraft should be maintained during the CRP, similar to such control of aircraft near airports, e.g., when scheduling landing [18].

Remark 6: Synchronization procedures needed to achieve a desired STA has been well studied in the literature, e.g., to schedule arrivals at airports [18], [19]. Such approaches can be adapted to manage asynchronous arrivals and achieve STAs for the CRP in a decentralized manner based on the arrival time, as shown in [1].

D. CRPs Are Decoupled

The path-split-based CRP satisfies decoupling conditions, as shown in [1], [3]. Briefly, equal-length paths (used in the CRP) enable the local procedure to satisfy the decoupling conditions provided that: 1) the aircraft arrival can be synchronized to the discrete time instants, and 2) the CRP avoids conflicts. The CRP does not change the sequence of aircraft in each route and maintains a minimal separation of $\overline{D}$ (i.e., the route-flow capacity for which the CRP is designed) at the exit. Therefore, if aircraft in one of the routes (R_1 or R_2) reaches another CP, then the CRP at the second intersection point does not have to depend on the procedures used at the first CRP provided the conflict points are sufficiently separated from each other, i.e., the associated local regions needed for conflict resolution are disjointed. Thus, the designs of the proposed distributed CRPs (which only uses local information of each route) can be decoupled from each other, without domino-type stability problems if the conflict points are sufficiently sparse in the airspace.

III. Conditions for Conflict Avoidance

The design of the CRP in Fig. 1 to ensure conflict avoidance between aircraft is studied in two parts: 1) the diverge procedure and 2) the intersect procedure. The converge procedure is the same as the diverge procedure backwards in time, and hence shares the same conflict avoidance issues. Therefore, the converge procedure is not discussed to avoid repetition.

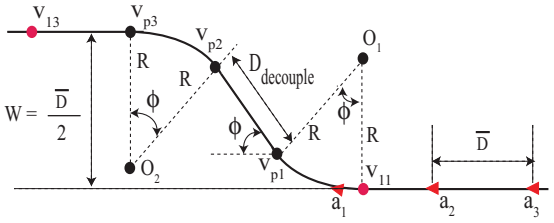

Fig. 2. Detail of path $R_{2,2}$ (v_{11} to v_{13} from Fig. 1) showing two turns.

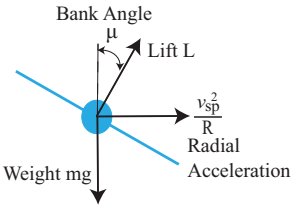

Fig. 3. Free body of aircraft performing a banked turn. The restriction on the acceptable bank angle limits the maximum heading-change rate.

A. Diverge Procedure

The different aspects of the diverge procedure (single turn, consecutive turns, and path splitting) are shown to be conflict-free below.

1) Potential for Conflicts During Turns: A critical concern is that the spacing between aircraft along a route could decrease during a turn (when compared to the arrival spacing $\overline{D}$ along each straight route) and result in the loss of minimum separation. Turns occur during the diverge procedure; e.g., in the path $R_{2,2}$ from Fig. 1, the route segment from v_{11} to v_{13} (diverge) consists of two consecutive turn paths each with constant radius R, and each curved path results in a heading angle change of ϕ as shown in Fig. 2. The potential for reduction in aircraft spacing during a turn places a lower limit on the initial spacing ($\overline{D}$) to achieve a turn ϕ without conflict. These restrictions can become more stringent when making consecutive turns. Conditions for conflict-free turns are studied below for two cases: 1) single turn, and 2) consecutive turns.

2) Restriction on Heading-Change Rate: Although the roll dynamics are relatively fast and can be ignored in the CRP path design, the aircraft turn dynamics should be included in terms of an upper bound on the heading-change rate $\dot{\theta}$ [2]. In particular, from the free-body diagram of the aircraft (in the vertical plane) shown in Fig. 3, the lift L and the bank angle μ are related by

$$L\cos(\mu) = mg, \quad L\sin(\mu) = mv_{\rm sp}^2/R \tag{4}$$

where $v_{\rm sp}$ is the nominal speed, m is the aircraft mass, and g is the gravitational acceleration. Then, the turn radius is given by $R = v_{\rm sp}^2/[g\tan(\mu)]$. With a bank angle limit of $\mu \le \mu_{\max}$ (where $\mu_{\max} = 30^\circ$ for passenger safety and comfort in commercial aircraft [2]), the minimum turn radius $R_{\min}$ is

$$R_{\min} = \frac{v_{\rm sp}^2}{g\tan(\mu_{\max})}. \tag{5}$$

The above lower bound on the turn radius, i.e., $R > R_{\min}$, leads to an upper bound on the maximum heading-change rate.

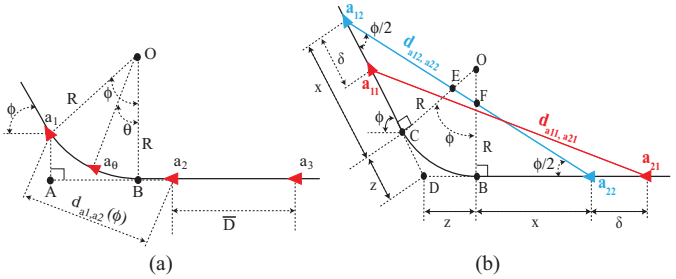

Fig. 4. (a) Single curved-turn case. (b) Distance between aircrafts during a single turn when only the forward aircraft has passed the curved path of the turn. Distance between the aircraft, $d_{a_{11},a_{21}}$, represents the nonequidistant case, and the distance $d_{a_{12},a_{22}}$ represents the symmetric equidistant case.

Let the aircraft make a heading change of $\theta \leq \phi$ in time t along a circular arc of radius R and length $R\theta = v_{\text{sp}}t$, as shown in Fig. 4(a). Then, the upper bound on the heading-change rate is obtained as

$$\dot{\theta} = \frac{v_{\text{sp}}}{R} \leq \frac{v_{\text{sp}}}{R_{\min}} = \frac{g\tan(\mu_{\max})}{v_{\text{sp}}} = \Omega_{\max}. \tag{6}$$

Thus, the limit on the acceptable bank angle implies that the turn rate should be bounded by a maximum value of $\Omega_{\max}$. Note that the rate of heading change $\dot{\theta}$ (i.e., the turn rate) can be kept below the upper bound of $\Omega_{\max}$ by choosing a sufficiently large turn radius R

$$R \geq R_{\min} = \frac{v_{\text{sp}}}{\Omega_{\max}}. \tag{7}$$

3) Single-Turn Analysis: Consider a single turn in a route where aircraft start from a straight section, then move along a circular arc of length $R\phi$, and finally continue along a straight line; both the straight line segments are tangential to the circular arc, and the angle between the two straight segments correspond to the turn angle ϕ as shown in Fig. 4(a).

Lemma 1 (Single Turn): To avoid conflict between aircraft on the route with the single curved turn [as in Fig. 4(a) with $R > R_{\min}$] and a maximum heading change of $\phi < \pi/2$, the minimum separation distance $\overline{D}$ between arriving aircraft (on the straight segment) should satisfy

$$\overline{D} \geq \overline{D}_{\phi} = \frac{D_{\text{sep}} - 2R\sin(\frac{\phi}{2})}{\cos(\frac{\phi}{2})} + R\phi \tag{8}$$

if $\phi \leq \phi^* = \frac{\overline{D}}{R}$, and

$$\overline{D} \geq \overline{D}_{\phi^*} = 2R\sin^{-1}\left(\frac{D_{\text{sep}}}{2R}\right) = \frac{(\phi^*/2)D_{\text{sep}}}{\sin(\phi^*/2)} \tag{9}$$

otherwise, i.e., when $\phi \geq \phi^*$. The two conditions are equivalent when the turn angle is the critical angle, i.e., $\phi = \phi^*$. Turn angle ϕ less than or equal to the critical angle ϕ^* will be referred to as scenario 1, and turn angle ϕ greater than the critical angle ϕ^* will be referred to as scenario 2.

Proof: The proof is divided into four steps.

Step 1 *(Distance Decreases During the Turn):* The distance between the forward aircraft a_1 and an aft aircraft a_2 that were separated by distance $\overline{D}$ in the straight portion decreases as aircraft a_1 starts turning along the circular arc while the aircraft a_2 is still on the straight path as in Fig. 4(a). To show this, consider the distance d_{a_1,a_2} between the two aircraft when the heading change of $\phi \leq \phi^*$ is completed by the first aircraft a_1, as in Fig. 4(a), given by

$$d_{a_1,a_2}(\phi) = \sqrt{(\overline{D} - R\phi + R\sin\phi)^2 + (R - R\cos\phi)^2} \tag{10}$$

if $\phi \leq \phi^*$, which follows from the right-angled triangle a_1Aa_2 because the length of the arc Ba_1 is $R\phi$, the path distance between the two aircraft is $\overline{D}$ due to the constant speed assumption, and, thereby, the distance $d_{B,a2}$ is $\overline{D} - $ âŁ"$R\phi$. If the turn angle θ completed by the aircraft a_1 satisfies $0 < \theta < \phi \leq \phi^*$, then the same expression holds with ϕ replaced by θ

$$d_{a_1,a_2}(\theta) = \sqrt{(\overline{D} - R(\theta - \sin\theta))^2 + (R - R\cos\theta)^2} \tag{11}$$

with the derivative of the distance squared given by

$$\frac{d}{d\theta}[d_{a_1,a_2}(\theta)]^2 = -2R\left(\overline{D} - R\theta\right)(1 - \cos\theta) < 0 \tag{12}$$

if $\theta \leq \phi < \phi^*$ and $\phi < \pi/2$ because $\overline{D} = R\phi^* \geq R\theta$—see definition of ϕ^* in (8). Thus, the distance d_{a_1,a_2} between the aircraft decreases as θ increases until $\theta = \phi \leq \phi^*$.

Step 2 (Minimum Distance for Scenario 2): The rate of change in distance with turn angle [the derivative in 12] becomes zero if $\theta = \phi^*$, which can occur if the desired heading-angle-change ϕ is greater than ϕ^*. The minimal distance reached when the turn angle becomes $\theta = \phi^*$ is given by (when $\phi \geq \phi^*$)

$$\begin{aligned} d_{a_1,a_2}(\phi^*) &= \sqrt{(R\sin\phi^*)^2 + (R - R\cos\phi^*)^2} \\ &= 2R\sin\tfrac{\overline{D}}{2R} = 2\tfrac{\overline{D}}{\phi^*}\sin\tfrac{\phi^*}{2}. \end{aligned} \tag{13}$$

It is noted that scenario 2 will be considered only if the critical angle ϕ^* is strictly less than $\pi/2$ to ensure the lemma's condition that the turn angle ϕ satisfies $\phi < \pi/2$. Furthermore, under scenario 2, when both aircraft are on the curved path, the distance between the aircraft is the minimum distance.

The minimum distance between the aircraft during the turn needs to be larger than the minimum required spacing D_{sep} to avoid conflict. Therefore, under scenario 2, from (13)

$$D_{\text{sep}} \leq d_{a_1,a_2}(\phi^*) = 2R\sin\tfrac{\overline{D}}{2R} = 2\tfrac{\overline{D}}{\phi^*}\sin\tfrac{\phi^*}{2} \tag{14}$$

which can be rewritten as (9) with arrival spacing $\overline{D} = D_{\phi^*}$ when the equality holds, i.e., $D_{\text{sep}} = d_{a_1,a_2}(\phi^*)$.

Step 3 *(Location for Minimum Distance for Scenario 1):* The following shows that the minimum distance between two aircraft occurs when both aircraft are on the straight-line segment, equidistant from the curved path. To show this, the distance $d_{a_{11},a_{21}}$ between aircraft a_{11} and a_{21} [general nonequidistant case, see Fig. 4(b)] is compared with the distance $d_{a_{12},a_{22}}$ between aircrafts a_{12} and a_{22} (symmetric equidistant case), where the distance between a_{12} and point C as well as a_{22} and point B is the same, x.

By geometry, the angle $\angle$CDB (shared by triangles $\triangle a_{11}Da_{21}$ and $\triangle a_{12}Da_{22}$) is $\pi - \phi$ since two of the angles in the quadrilateral CDBO are $\pi/2$. Then, the distances between the aircraft, $d_{a_{11},a_{21}}$ (nonequidistant case) and $d_{a_{12},a_{22}}$

(symmetric equidistant case), can be found by using the law of cosines as shown below

$$\begin{aligned} d_{a_{11},a_{21}}^2 &= d_{D,a_{11}}^2 + d_{D,a_{21}}^2 - 2d_{D,a_{11}}d_{D,a_{21}}\cos(\pi-\phi) \\ &= (x+z-\delta)^2 + (x+z+\delta)^2 \\ &\quad -2(x+z-\delta)(x+z+\delta)\cos(\pi-\phi) \\ &= 2(x+z)^2(1+\cos(\phi)) + 2\delta^2(1-\cos(\phi)) \quad (15) \\ d_{a_{12},a_{22}}^2 &= d_{D,a_{12}}^2 + d_{D,a_{22}}^2 \\ &\quad -2d_{D,a_{12}}d_{D,a_{22}}\cos(\pi-\phi) \\ &= (x+z)^2 + (x+z)^2 \\ &\quad -2(x+z)(x+z)\cos(\pi-\phi) \\ &= 2(x+z)^2\left[1+\cos(\phi)\right]. \quad (16) \end{aligned}$$

The differences between the two distances, the nonequidistant case and the symmetric equidistant case, can be found by subtracting (15) from (16) to obtain

$$d_{a_{11},a_{21}}^2 - d_{a_{12},a_{22}}^2 = 2\delta^2(1-\cos\phi) \geq 0. \quad (17)$$

Therefore, from (17), the symmetric equidistant case has the smallest distance for aircraft pairs during the single-turn case under scenario 1.

Step 4 (Minimum-Distance Expression for Scenario 1): For the symmetric equidistant case in Fig. 4 (b), the minimum distance during the turn $d_{a_{12},a_{22}}$ (between aircraft positions a_{12} and a_{22}) can be found by adding the three distances $d_{a_{12},E}$, $d_{E,F}$, and $d_{a_{22},F}$, which are found below. Note that, by symmetry, distance $d_{a_{12},E}$ is the same as distance $d_{a_{22},F}$.

Note that the travel distance between a_{12} and a_{22} is $\overline{D}$. Since the arc length of the turn between point B and point C in Fig. 4(b) is $R\phi$, the distance x is found to be $0.5(\overline{D}-R\phi)$. Because of the symmetry in geometry, $\triangle OEF$ is an isosceles triangle. Since $\angle EOF$ is the turn angle ϕ, the angles $\angle a_{12}EC$ and $\angle Ea_{12}C$ are found as $\pi/2-\phi/2$ and $\phi/2$, respectively. From the right-angled triangle $\triangle Ea_{12}C$

$$d_{C,E} = d_{B,F} = \frac{1}{2}\tan(\phi/2)(\overline{D}-R\phi) \quad (18)$$

$$d_{a_{12},E} = d_{a_{22},F} = \frac{1}{2}\frac{\overline{D}-R\phi}{\cos(\phi/2)}. \quad (19)$$

Since the distances $d_{O,C}$, $d_{O,B}$ are the turn radius R, from (18)

$$d_{O,E} = d_{O,F} = R - d_{C,E} = R - \frac{\tan(\frac{\phi}{2})(\overline{D}-R\phi)}{2}. \quad (20)$$

Next, from $\triangle OEF$, the distance $d_{E,F}$ between points E and F can be found by using the law of sines as

$$\frac{d_{E,F}}{\sin\phi} = \frac{d_{O,E}}{\sin(\pi/2-\phi/2)}. \quad (21)$$

Substituting for distance $d_{O,E}$ from (20) into the above equation leads to

$$\begin{aligned} d_{E,F} &= \left[R - \frac{1}{2}\tan(\phi/2)(\overline{D}-R\phi)\right]\frac{\sin(\phi)}{\sin(\pi/2-\phi/2)} \\ &= 2R\sin(\phi/2) - \frac{\sin^2(\phi/2)}{\cos(\phi/2)}(\overline{D}-R\phi). \quad (22) \end{aligned}$$

Then, the minimal spacing between aircraft can be found as [from (19) and (22)]

$$\begin{aligned} d_{a_{12},a_{22}} &= d_{a_{12},E} + d_{E,F} + d_{a_{22},F} \\ &= (\overline{D}-R\phi)\cos(\phi/2) + 2R\sin(\phi/2) \quad (23) \end{aligned}$$

which results in the condition [in 8] for scenario 1 of the Lemma by setting $d_{a_{12},a_{22}} \geq D_{\text{sep}}$ in (23) and rearranging the terms. ■

4) Conflict-Free Consecutive Turns: A general conflict resolution algorithm could have multiple consecutive turns, e.g., during the diverge/converge procedure. The conflict-free single-turn analysis can be used to show the existence of conflict-free multiple turns provided each turn is sufficiently separated from each other. In particular, sufficient spacing between the turns allows conflict-free consecutive turns, leading to an offset in the aircraft path during the converge and diverge procedure, as shown in Fig. 2.

Definition 3 [Path Offset Maneuver]: The offset maneuver, shown in Fig. 2, consists of two consecutive turns of a route where the aircraft start from a straight section, then move along a circular arc (with arc length of $R\phi$, $0 < \phi < \pi/2$), followed by a straight decoupling section, a turn again in the opposite direction (with arc length of $R\phi$), and finally a turn into a straight section. The initial and final straight-line sections are parallel, leading to a path-offset maneuver. Moreover, all the straight segments are tangential to the curved paths to avoid large heading-change rates.

Lemma 2 (Path Offset Maneuver is Conflict-Free): If conditions of the single-turn Lemma 1 are satisfied for each of the turns inside the consecutive turn maneuver shown in Fig. 2, then the offset maneuver (with consecutive turns) is conflict-free as long as the straight decoupling section—in between the two turns—is sufficiently large.

Proof: The proof follows from Lemma 1 because a sufficiently large straight line segment $\overline{v_{p1}, v_{p2}}$ (e.g., of length $D_{\text{decouple}} > \overline{D}$) in the middle of the consecutive turn (in Fig. 2) implies that there will be no conflicts between aircraft on the two different curved segments (in Fig. 2). Therefore, the straight segment in the middle decouples potential conflicts in the maneuver into those for two decoupled single turns, which are conflict-free from Lemma 1. ■

Remark 7: The straight-line section of length D_{decouple} in Fig. 2 between the turns is only used to establish the existence of a conflict-free solution. In practice, the length of this straight line section can be reduced to decrease the space needed for the path-offset maneuver.

Remark 8: The above lemma can be used to establish the arrival rate criteria for other CRP procedures (e.g., [12]) that use such offset maneuvers.

5) Conflict-Free Path Splitting:

Lemma 3: Without splitting, let there be no conflicts along a path that is to one side of the initial straight line segment as in Fig. 5. Then, there are no conflicts with the path splitting if it is symmetric about the axis of the initial straight line segment.

Proof: Since there is no conflict between aircraft without the path splitting, the distance between aircraft locations a_1, a_2

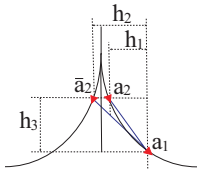

Fig. 5. Potential conflict between aircraft during path splitting.

in Fig. 5 is greater than the minimal separation distance, i.e., $d_{a_1,a_2} \geq D_{\text{sep}}$. This implies that there are no conflicts even if the two aircraft were on diverging paths, e.g., between aircraft locations $a_1, \bar{a}_2$ in Fig. 5, because

$$d_{a_1,\bar{a}_2} = \sqrt{h_3^2 + h_2^2} \geq \sqrt{h_3^2 + h_1^2} = d_{a_1,a_2} \geq D_{\text{sep}} \qquad (24)$$

where $h_2 \geq h_1$ because aircraft locations a_2 and $\bar{a}_2$ are on two sides of the axis of the initial straight line segment. ■ This completes the arguments to show that the different parts of the diverge procedure are conflict-free.

B. Flow Intersect Procedure

The minimum spacing between aircraft needed to enable a single conflict-free intersection is considered next.

Lemma 4: Let the aircraft arrive at a perpendicular intersection evenly spaced in each path at distance $d_{\pi/2}$. Moreover, when an aircraft from one of the paths is at the intersection, it is centered between the aircraft from the other path with a minimal distance of $0.5d_{\pi/2}$. Then, for a conflict-free perpendicular intersection, the minimal spacing in each path is

$$d_{\pi/2} = 2\sqrt{2}D_{\text{sep}}. \qquad (25)$$

Proof: Consider the case in Fig. 6(a) where aircraft a_1 from route $R_{1,1}$ has advanced a distance x from the intersection. Then, the separation distance $d_{a1,b2}$ between aircraft a_1 (on path $R_{1,1}$) and b_2 (on path $R_{2,1}$) is given by

$$\begin{aligned} d_{a1,b2}^2 &= \left(\frac{d_{\pi/2}}{2} - x\right)^2 + x^2 \\ &= \left[\sqrt{2}x - \frac{d_{\pi/2}}{2\sqrt{2}}\right]^2 + \frac{d_{\pi/2}^2}{8}. \end{aligned} \qquad (26)$$

The minimal distance $d_{a1,b2,min}$ between aircraft $d_{a1,b2}$ (over all x) needs to be larger than the minimal separation distance of D_{sep}, i.e., $d_{a1,b2,min}^2 = d_{\pi/2}^2/8 \geq D_{\text{sep}}^2$

which results in the condition 25 in the lemma] for the minimal spacing between aircraft in each path. ■

Splitting the routes into n paths increases the spacing between aircraft from $\overline{D}$ in each route to $n\overline{D}$ in each path, which enables conflict-free intersections from Lemma 4.

Lemma 5: Aircraft that arrive synchronized do not have conflicts with each other in the intersection area (e.g., marked by D_i in Fig. 1 for route R_1) with the use of the two-path assignment procedure in Definition 2 if the path lengths from the arrival points to the straight-line segments are all equal and $2\overline{D} > 2\sqrt{2}D_{\text{sep}} = d_{\pi/2}$.

Proof: This follows from Lemma 4 and [1] since all scenarios under which an aircraft can occupy a path intersection in Fig. 6 (b) satisfy Lemma 4 conditions. ■

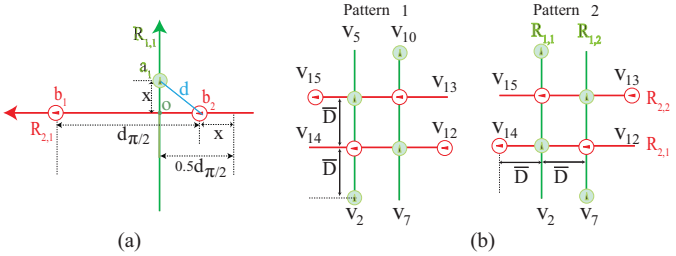

Fig. 6. (a) Separation distance on a single intersection. (b) All possible scenarios under which an aircraft can occupy a path intersection in Fig. 1.

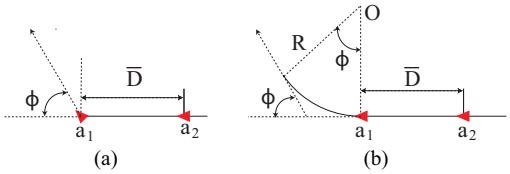

Fig. 7. (a) Rate-unbounded (instantaneous) turn. (b) Rate-bounded turns.

Remark 9: [Number of paths splits] The number n of paths required is at most 3 since the resulting aircraft spacing on the paths will satisfy Lemma 4 condition, i.e., $3\overline{D} > 2\sqrt{2}D_{\text{sep}}$ as the minimal arrival spacing $\overline{D}$ is larger than the minimal separation distance D_{sep}. CRPs with more than two splits have been studied in [1], [3]. Increasing the number of splits can increase the minimal aircraft distance in the CRP and, therefore, enhance the robustness of the CRP.

This completes the discussion to show that the proposed CRP is conflict-free provided the arrival spacing conditions are met for the single turn (Lemma 1) and consecutive turns are sufficiently separated (Lemma 2).

IV. Bounded Versus Unbounded Rate Turns

The rate-bounded (continuous) turn and the rate-unbounded (instantaneous) turn, shown in Fig. 7, are comparatively evaluated to illustrate the importance of including the turn dynamics in the CRP design.

A. Importance of Single-Turn Analysis

The arrival-spacing requirement to have a conflict-free single-turn (in Lemma 1) is the critical requirement for the proposed conflict-free CRP design. This is because conflict-free conditions for multiple turns (in the converge and diverge portions of the CRP) can be established using the single-turn condition as shown in Lemmas 2 and 3. Moreover, the flow-intersect procedure does not add requirements on the route's arrival spacing since sufficient spacing for conflict-free intersection can be achieved by splitting each route into at the most three paths as in Remark 9. Therefore, the arrival spacing requirement for the overall CRP can be established using Lemma 1, which develops the conditions to avoid conflicts within a single turn.

B. Comparison of Arrival Spacing

Lemma 6: For any given turn angle $0 < \phi < \pi/2$, the lower bound (e.g., $\overline{D}_\phi$ in 8, Lemma 1) on the acceptable arrival-spacing distance $\overline{D}$ for a rate-bounded turn maneuver is less

than the corresponding lower bound ($\overline{D}_{\phi,\text{inst}}$) on the acceptable arrival-spacing distance $\overline{D}$ for an instantaneous turn maneuver.

Proof: The lower bound $\overline{D}_{\phi,\text{inst}}$ on the acceptable arrival-spacing distance $\overline{D}$ for an instantaneous turn is given by [1]

$$\overline{D}_{\phi,\text{inst}} = \frac{D_{\text{sep}}}{\cos(\phi/2)}. \tag{27}$$

For scenario 1 ($\phi \le \phi^*$ in Lemma 1), the difference between the lower bounds for the two cases (instantaneous turn versus rate-bounded turn) is, from (8) and (27)

$$\begin{aligned}\overline{D}_{\phi,\text{inst}} - \overline{D}_{\phi} &= \frac{D_{\text{sep}}}{\cos(\phi/2)} - \left[\frac{D_{\text{sep}} - 2R\sin(\phi/2)}{\cos(\phi/2)} + R\phi\right] \\ &= R\left[2\tan(\phi/2) - \phi\right] \quad = R\Delta_{\overline{D}}(\phi).\end{aligned} \tag{28}$$

The Lemma follows for scenario 1 ($\phi \le \phi^*$) since

$$\Delta_{\overline{D}}(\phi) = \int_0^{\phi/2} \frac{d\Delta_{\overline{D}}}{d\phi} d\phi = \int_0^{\phi/2} \tan^2(\phi/2) d\phi > 0 \tag{29}$$

where the integrand is a positive continuous function when $\phi > 0$.

For scenario 2 ($\phi > \phi^*$ in Lemma 1), the difference between the lower bounds for the two cases (instantaneous turn versus rate-bounded turn) is, from (9) and (27)

$$\begin{aligned}\overline{D}_{\phi,\text{inst}} - \overline{D}_{\phi^*} &= \frac{D_{\text{sep}}}{\cos(\phi^*/2)} - (R\phi^*) \\ &= R\left[2\tan(\phi^*/2) - \phi^*\right] \text{ from Eq. (14)} \\ &= R\Delta_{\overline{D}}(\phi^*).\end{aligned} \tag{30}$$

The Lemma follows for scenario 2 ($\phi > \phi^*$) since $\Delta_{\overline{D}}(\phi^*) > 0$ from (29) because $\phi^* < \phi < \pi/2$. ■

Remark 10: The above Lemma also implies that a larger turn angle ϕ is possible with a given aircraft spacing $\overline{D}$ for the rate-bounded approach when compared to the instantaneous-turn case. This is to be expected because the rate-bounded turn takes more distance to complete the turn when compared to the instantaneous turn (see Fig. 7). Therefore, the reduction of aircraft spacing during the more gradual rate-bounded turn is expected to be less, leading to less potential for conflict.

Lemma 7 (Effect of Increasing the Turn Radius): For a given arrival spacing $\overline{D} > D_{\text{sep}}$, the rate-bounded turn can achieve any given turn angle $0 < \phi < \pi/2$ with a sufficiently large turn radius R.

Proof: The rate-bounded turn becomes a scenario 2 case (i.e., $\phi^* < \phi$) for a sufficiently large turn radius R since, from (8), the critical turn angle ϕ^* becomes small ($\phi^* \to 0$) as the turn radius increases ($R \to \infty$). As a result, from (9), the minimal arrival spacing $\overline{D}_{\phi^*}$ scenario 2 tends to the limit

$$\lim_{\phi^* \to 0} \overline{D}_{\phi^*} = \lim_{\phi^* \to 0} \frac{D_{\text{sep}}\phi^*/2}{\sin(\phi^*/2)} = D_{\text{sep}} \tag{31}$$

as the turn radius increases ($R \to \infty$). Then, the arrival flow spacing distance $\overline{D}$ is greater than the minimal arrival spacing distance $\overline{D}_{\phi^*}$ for a sufficiently large turn radius R because

$$\begin{aligned}\lim_{R \to \infty} \overline{D} - \overline{D}_{\phi^*} &= \lim_{\phi^* \to 0} \left[(\overline{D} - D_{\text{sep}}) - (\overline{D}_{\phi^*} - D_{\text{sep}})\right] \\ &= \overline{D} - D_{\text{sep}} \ > 0.\end{aligned} \tag{32}$$

■

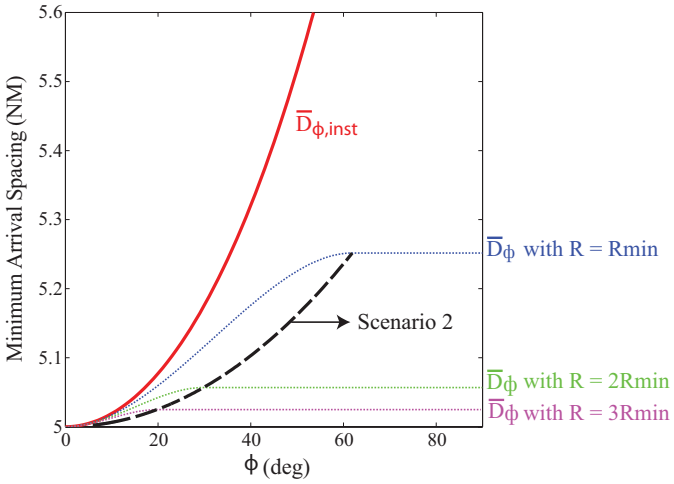

Fig. 8. Comparison of minimum arrival spacing for rate-bounded turns $\overline{D}_{\phi}$ from (8) and (9) (dotted lines) and instantaneous turns $\overline{D}_{\phi,\text{inst}}$ from (27) (solid line).

The lower bound on the minimal arrival spacing is compared in Fig. 8. As expected from Lemma 6, for a given turn angle ϕ, the rate-bounded turn can be achieved with a lower arrival spacing when compared to the instantaneous case. Moreover, Fig. 8 shows that the maximum allowable turn angle is larger with the rate-bounded turn when compared to the single instantaneous turn. Furthermore, as the turn radius is increased, e.g., from $R = R_{\text{min}}$ to $R = 2R_{\text{min}}$, the required arrival spacing decreases. While any turn angle $0 < \phi < \pi/2$ can be achieved for any given arrival spacing $\overline{D} > D_{\text{sep}}$ with a rate-bounded turn (by choosing a sufficiently large turn radius R), the maximum turn angle ϕ is limited for the instantaneous case to $\phi < 2\cos^{-1}\left(D_{\text{sep}}/\overline{D}\right)$ according to (27).

For example, with an arrival spacing of $\overline{D} = 5.1$ NM, the maximum turn angle for the instantaneous turn is $\phi = 22.73^{\circ}$, as seen in Fig. 8. Even for the instantaneous turn case, multiple turns can be used to achieve a larger net turn $0 < \phi < \pi/2$; however, each turn would not be consistent with the aircraft turn-rate bounds. In contrast, by choosing a sufficiently large turn radius, e.g., $R = 2R_{\text{min}}$, any turn angle $0 < \phi < \pi/2$ can be achieved with the rate-bounded approach. Thus, the above development of rate-bounded turns enables the design of CRPs, which include the aircraft turn dynamics.

V. Example Route Intersection

An example route intersection is used in this section to illustrate the CRP design. Additionally, robustness of the proposed CRP is discussed.

A. Description of the Route Intersection

Conflicts are not expected in existing aircraft data (since these are already resolved); however, existing data can be used to illustrate issues in the design of the proposed CRP. In particular, data from a perpendicularly intersecting route in the Cleveland sector ZOB59 (see Fig. 9) was used to: 1) quantify the minimum arrival spacing $\overline{D}_{\text{min}}$ in the routes, and 2) identify the average aircraft velocity and its variation.

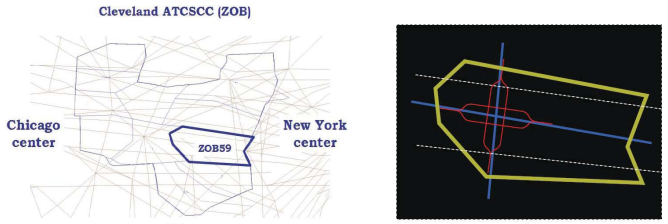

Fig. 9. (a) Cleveland sector ZOB59. (b) Perpendicularly intersecting routes (solid line), CRP designed with the arrival spacing of $\overline{D} = 9.23$ NM, and example nearby routes (dashed lines).

The data was obtained using the Future ATM Concepts Evaluation Tool (FACET) for May 1, 2004 at 35 000 ft altitude during the time interval [305, 65 735] Coordinated Universal Time (UTC) seconds, which corresponds to about 18 h of data. During this period, 35 aircraft passed through the east-to-west route, and 19 aircraft passed through the north-to-south route. The average velocity of these aircraft on the two routes from Fig 9 was 0.122 NM/s (nautical miles per second) with a standard deviation of 0.005 NM/s. The minimum spacing between aircraft pairs was $\overline{D}_{\min} = 9.23$ NM.

B. CRP Design

The design variables in the CRP design are the arrival spacing $\overline{D}$, the number of paths into which the routes are split, the turn angle ϕ, and the turn radius R in the converge/diverge procedures.

1) Bounds on Arrival Spacing: A smaller number of split paths (of each route) can reduce the overall area needed for the CRP. The maximum possible arrival spacing $\overline{D}$ that can be used in the CRP design is the minimal aircraft spacing in the routes $\overline{D}_{\min} = 9.23$ NM, for this example

$$\overline{D} \leq \overline{D}_{\min} = 9.23\ NM. \tag{33}$$

The maximum arrival spacing $\overline{D} = 9.23$ NM is still smaller than the spacing needed $2\sqrt{2}D_{\text{sep}} = 14.14$ NM for the conflict-free intersection condition from (25) in Lemma 4, where the minimal separation distance is $D_{\text{sep}} = 5$ NM. Therefore, each route needs to be split into at least two paths as in Fig. 6. With two paths, the possible choice of arrival spacing $\overline{D}$ needs to satisfy, from Lemma 4

$$2\overline{D} \geq 2\sqrt{2}D_{\text{sep}} = 14.14\ NM. \tag{34}$$

From (33) and (34), the acceptable arrival spacing $\overline{D}$ in the CRP design should satisfy

$$\frac{2\sqrt{2}}{2}D_{\text{sep}} = 7.07(NM) \leq \overline{D} \leq \overline{D}_{\min} = 9.23(NM). \tag{35}$$

2) Turn Angle and Radius: During the diverge section (and similarly during the converge section), e.g., between nodes v_1 and v_2 in Fig. 1, the route is offset by half the arrival spacing $\overline{D}/2$ used in the CRP design by using the path-offset scheme shown in Fig. 2. Moreover, to minimize the space needed for the maneuver, we begin with the smallest possible decoupling distance, $D_{\text{decouple}} = 0$. Minimal separation between aircraft with this choice needs to be checked numerically, however.

The analysis in Section III shows that the CRP will be safe provided the decoupling distance is sufficiently large. With a zero decoupling distance $D_{\text{decouple}} = 0$, the offset requirement implies that

$$\overline{D}/2 = 2R(1 - \cos\phi) \tag{36}$$

which relates the turn radius R and the turn angle ϕ by

$$R = \frac{\overline{D}/4}{1 - \cos\phi}. \tag{37}$$

3) Choosing the Turn Angle: The lateral distance L_{curve} needed for the offset maneuver with bounded-rate turns (see Fig. 2) is given by (with zero decoupling distance $D_{\text{decouple}} = 0$)

$$L_{\text{curve}} = 2R\sin\phi = \frac{\overline{D}/2}{1 - \cos\phi}\sin\phi. \tag{38}$$

Note that the required lateral distance L_{curve} decreases with increasing turn angle ϕ (for $0 < \phi < \pi/2$) since the derivative with respect to ϕ is negative

$$\begin{aligned}\frac{dL_{\text{curve}}}{d\phi} &= \frac{\overline{D}}{2}\left[\frac{\cos\phi(1 - \cos\phi) - \sin^2\phi}{(1 - \cos\phi)^2}\right] \\ &= -\frac{\overline{D}}{2}\left[\frac{1}{(1 - \cos\phi)}\right] \leq 0.\end{aligned} \tag{39}$$

Therefore, the turn angle ϕ should be chosen as large as possible to reduce the lateral distance L_{curve} needed to accomplish the offset maneuver, which, in turn, will reduce the overall space needed for the CRP. However, the required turn radius R [from (37)], which needs to be larger than the minimum turn radius [$R_{\min}$ from (7)], decreases with increasing turn angle ϕ for $0 < \phi < \pi/2$ since the denominator in (37) is increasing with ϕ. The maximum turn angle $\phi = \phi_{\max}$, which occurs when $R = R_{\min}$, can be found from (37) as

$$\phi_{\max} = \cos^{-1}\left[1 - \frac{\overline{D}}{4R_{\min}}\right]. \tag{40}$$

4) Effect of Varying the Arrival Spacing: The minimal distance $D_{\text{cd,min}}$ between aircraft during the diverge maneuver and the minimal distance $D_{\text{i,min}}$ during the intersect portion of the CRP are computed numerically and shown in Fig. 10 for different values of the arrival spacing $\overline{D}$ in the acceptable range from (35) with zero decoupling distance $D_{\text{decouple}} = 0$. The overall minimal distance in the CRP is at least the minimal separation distance D_{sep}, and, therefore, the CRP is conflict-free for arrival spacing $\overline{D}$ in the acceptable range (35), even with zero decoupling distance $D_{\text{decouple}} = 0$. The minimal distance between the aircraft in the CRP increases with the arrival spacing $\overline{D}$ used in the design.

The variation of the size D_{CRP} of the CRP (see Fig. 1), given by

$$\begin{aligned}D_{\text{CRP}} &= 2D_{cd} + D_i \\ &= 2\frac{\overline{D}/2}{1 - \cos\phi_{\max}}\sin\phi_{\max} + 3\overline{D}\end{aligned} \tag{41}$$

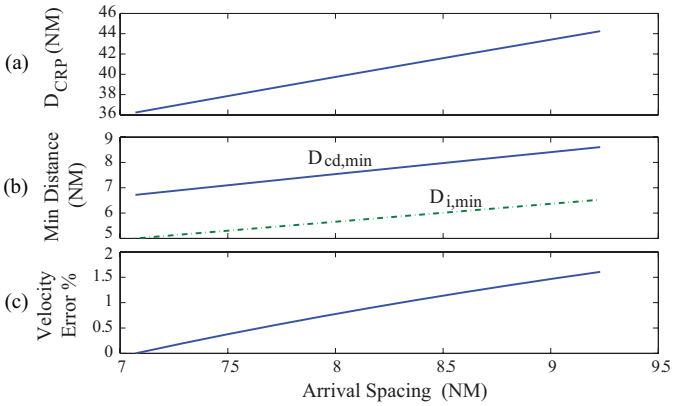

Fig. 10. Effect of choosing different arrival spacing $\overline{D}$ in CRP design. (a) Variation of the CRP size D_{CRP} from (41). (b) Variation of the minimal distance $D_{\text{cd,min}}$ in the converge/diverge section and the minimal distance $D_{\text{i,min}}$ in the intersect section. (c) Variation of percent acceptable velocity error $E_{v,\%}$ from (43).

is shown in Fig. 10. The space needed for the CRP (quantified by D_{CRP}) increases with the arrival spacing $\overline{D}$ used in the design.

Remark 11: A CRP with smaller space requirement will enable more dense route structures, e.g., comparison of space needed in Fig. 10. In general, a redesign of the overall route structure will be needed to provide sufficient space when adopting the proposed CRP approach. For example, nearby routes (e.g., shown in dashed lines in Fig. 9) will need to be spaced further away. Alternatively, resolution of nearby conflicts can be integrated into a compound CRP [1].

C. Size Versus Robustness

Using a smaller arrival spacing leads to a smaller CRP size (quantified by D_{CRP}); however, it also leads to lower robustness as shown below. In particular, the space needed for the CRP is minimized by choosing the smallest arrival spacing $\overline{D} = (2\sqrt{2}/2)D_{\text{sep}} = 7.07$ NM, as seen in Fig. 10. However, this design is not robust since the minimal distance of aircraft in the CRP is equal to the minimum required aircraft separation $D_{\text{sep}} = 5$ NM from Fig. 10. For example, small variations, e.g., in the speed of the aircraft, can lower distance between the aircraft below the required aircraft separation D_{sep}, leading to conflicts between aircraft.

In contrast, with the larger arrival spacing $\overline{D} = 9.23$ NM, the minimal distance between the aircraft in the CRP (which occurs in the intersection region as shown in Fig. 10) is given by $D_{\text{i,min}} = 9.23/\sqrt{2} = 6.5266$ NM. This larger than the minimal required separation leads to robustness of the CRP, for example, due to errors caused by velocity variations. To illustrate, let the maximum path length for aircraft through the CRP be P_{CRP} given by

$$\begin{aligned} P_{\text{CRP}} &= 4R\phi_{\max} + 3\overline{D} \\ &= 4\frac{\overline{D}/4}{1-\cos\phi_{\max}}\phi_{\max} + 3\overline{D}. \end{aligned} \tag{42}$$

Then, the maximum error e_{pos} in the position of an aircraft (from the expected position with the nominal speed v_{sp} during the CRP is $e_{\text{pos}} = P_{\text{CRP}}\delta_{\text{vmax}}/v_{sp}$ where δ_{vmax} is the maximum (absolute) deviation from the nominal velocity. This position error would be acceptable during the CRP, if it does not lead to conflict. Since each aircraft could have velocity deviations, the resulting error in position e_{pos} of each aircraft needs to be smaller than half the excess separation between aircraft in the CRP, i.e., $e_{\text{pos}} \leq (D_{i,\min} - D_{\text{sep}})/2$. Therefore, the acceptable variation in the aircraft speed is

$$E_{v,\%} = \frac{\delta_{\text{vmax}}}{v_{\text{sp}}} * 100 \leq \frac{D_{i,\min} - D_{\text{sep}}}{2P_{\text{CRP}}} \times 100 \tag{43}$$

which increases with an increase in the arrival spacing $\overline{D}$ used the CRP design, as seen in Fig. 10. For the example, with the maximum arrival spacing $\overline{D} = 9.23$ NM, the velocity error needs to be maintained below 1.6% to avoid conflicts.

Remark 12: Even for the smallest arrival spacing of $\overline{D} = 7.07$ NM, the CRP can be redesigned to be robust by including a factor of safety K_{fs} in the minimum separation distance D_{sep} between aircraft used in the CRP design, i.e., by choosing a larger minimum separation distance $\overline{D}_{\text{sep}} = K_{\text{fs}}D_{\text{sep}}$. The resulting excess separation $(\overline{D}_{\text{sep}} - D_{\text{sep}})$ can be used to ensure robustness.

VI. Conclusion

This brief presented a CRP that includes the effect of turn dynamics by bounding the heading-change (turn) rate. The main importance of including the turn-rate bound is when proving the existence of a safe CRP. In particular, as shown in Section IV, for a given arrival spacing $\overline{D}$ in the intersecting routes, the allowable turn angle (in a single turn) can be different depending on wether the turn-rate bound is included in the analysis or not. The bounded turn analysis (with a given arrival spacing $\overline{D}$) is important to establish the existence of conflict-free converge/diverge procedures in Section III. Moreover, the bounded turn-rate analysis is important to quantify the size of the converge/diverge procedure and, therefore, to quantify the space needed for the CRP. The proposed CRP was illustrated with an example conflict between two routes in the Cleveland sector.

This brief was aimed at establishing the existence of decoupled CRP, which is challenging, in general, for large distributed systems such as ATC. However, additional work is needed to optimize the CRP, e.g., to minimize the time delay generated by the CRP. Moreover, efforts are needed to remove some of the limitations of the proposed approach, such as the need to maintain the CRP even when there are no conflicts. Our current efforts are aimed at developing conditions for activating the CRP when needed and removing it when conflicts are not present. Future work should also consider issues such as extension of the proposed CRP for nonperpendicular intersections, time-varying flow rates in the routes, and large variations in aircraft speeds.

Acknowledgment

The authors would like to thank Dr. D. Iamratanakul for data extraction for the example problem.

REFERENCES

[1] S. Devasia, D. Iamratanakul, G. Chatterji, and G. Meyer, "Decoupled conflict-resolution procedures for decentralized air traffic control," *IEEE Trans. Intell. Trans. Syst.*, vol. 12, no. 2, pp. 422–437, Jun. 2011.

[2] J. Krozel, C. Lee, and J. S. B. Mitchell, "Turn-constrained route planning for avoiding hazardous weather," *Air Traff. Control Quart.*, vol. 14, no. 2, pp. 159–182, 2006.

[3] J. Yoo and S. Devasia, "Flow-capacity-maintaining, decentralized, conflict resolution with aircraft turn dynamics," in *Proc. Amer. Control Conf.*, Jul. 2011, pp. 2759–2764.

[4] J. Yoo and S. Devasia, "Application of provably-safe conflict resolution for air traffic control," in *Proc. Conf. Decision Control*, Dec. 2012, pp. 1–7.

[5] M. Prandini, L. Piroddi, S. Puechmorel, and S. L. Brazdilova, "Toward air traffic complexity assessment in new generation air traffic management systems," *IEEE Trans. Intell. Trans. Syst.*, vol. 12, no. 3, pp. 809–818, Sep. 2011.

[6] A. Haraldsdottir, R. W. Schwab, and M. S. Alcabin, "Air traffic management capacity-driven operational concept through 2015," in *Proc. 2nd Int. Air Traff. Manag. RD Seminar, Sponsored US Federal Aviat. Administrat.*, Dec. 1998, pp. 706–741.

[7] Y. Wan and S. Roy, "A scalable methodology for evaluating and designing coordinated air-traffic flow management strategies under uncertainty," *IEEE Trans. Intell. Trans. Syst.*, vol. 9, no. 4, pp. 644–656, Dec. 2008.

[8] W. B. Cotton, "Formulation of the air traffic system as a management problem," *IEEE Trans. Commun.*, vol. 21, no. 5, pp. 375–382, May 1973.

[9] K. D. Bilimoria, K. S. Seth, H. Q. Lee, and S. R. Grabbe, "Performance evaluation of airborne separation assurance for free flight," in *Proc. AIAA Guid. Navigat. Control Conf.*, Aug. 2000, pp. 1–9.

[10] A. L. Visintini, W. Glover, J. Lygeros, and J. Maciejowski, "Monte carlo optimization for conflict resolution in air traffic control," *IEEE Trans. Intell. Trans. Syst.*, vol. 7, no. 4, pp. 470–482, Dec. 2006.

[11] L. Pallottino, E. M. Feron, and A. Bicchi, "Conflict resolution problems for air traffic management systems solved with mixed integer programming," *IEEE Trans. Intell. Trans. Syst.*, vol. 3, no. 1, pp. 3–11, Mar. 2002.

[12] Z.-H. Mao, D. Dugail, E. Feron, and K. Bilimoria, "Stability of intersecting aircraft flows using heading-change maneuvers for conflict avoidance," *IEEE Trans. Intell. Trans. Syst.*, vol. 6, no. 4, pp. 357–369, Dec. 2005.

[13] C. Tomlin, I. Mitchell, and R. Ghosh, "Safety verification of conflict resolution maneuvers," *IEEE Trans. Intell. Trans. Syst.*, vol. 2, no. 2, pp. 110–120, Jun. 2001.

[14] Z.-H. Mao, D. Dugail, and E. Feron, "Space partition for conflict resolution of intersecting flows of mobile agents," *IEEE Trans. Intel. Trans. Sys.*, vol. 8, no. 3, pp. 512–527, Sep. 2007.

[15] S. Devasia and G. Meyer, "Automated conflict resolution procedures for air traffic management," in *Proc. 36th Conf. Decision Control, Phoenix, AZ*, Dec. 1999, pp. 2456–2462.

[16] A. M. Bayen, R. L. Raffard, and C. J. Tomlin, "Adjoint-based control of a new eulerian network model of air traffic flow," *IEEE Trans. Control Syst. Technol.*, vol. 14, no. 5, pp. 804–818, Sep. 2006.

[17] J. Prete, J. Krozel, J. Mitchell, J. Kim, and J. Zou, "Flexible, performance-based route planning for super-dense operations," in *Proc. AIAA Guid. Navigat. Control Conf.*, Aug. 2008, pp. 1–14.

[18] H. Erzberger and W. Nedell, "Design of automated system for management of arrival traffic," in *Proc. NASA Tech. Memo.*, Jun. 1989, pp. 1–6.

[19] Y. Eun, I. Hwang, and H. Bang, "Optimal arrival flight sequencing and scheduling using discrete airborne delays," *IEEE Trans. Intell. Trans. Syst.*, vol. 11, no. 2, pp. 359–373, Mar. 2010.